Real-Time and Background-Free Detection of Nanoscale Particles

Filipp V. Ignatovich and Lukas Novotny*

The Institute of Optics, University of Rochester, Rochester, New York 14627, USA†

(Received 9 August 2005; published 3 January 2006)

We introduce a background-free real-time detection scheme capable of recognizing low-index nanoparticles such as single viruses in water. The method is based on interferometrically measuring the electromagnetic field amplitude of the scattered light. A split detector is used to generate a background-free signal that renders unprecedented sensitivity for small particles. In its current configuration the sensor is capable of detecting low-index particles in water down to 10 nm in radius or single gold particles as small as 5 nm. We demonstrate the detection of such small particles in a microfluidic system with a time resolution of 1 ms and we discuss the theoretical limits of this novel detection scheme.

DOI: 10.1103/PhysRevLett.96.013901 PACS numbers: 42.90.+m, 87.64.Cc, 87.64.Rr

Particles with characteristic sizes of less than 100 nm are becoming increasingly important in the context of nanoscience and technology. Applications range from solid-state physics to biology. For example, semiconductor nanoparticles are used as single photon emitters in quantum information science [1] and as fluorescent markers for biological processes [2]. Similarly, noble metal particles are used as contrast agents in microscopy [3], as biochemical sensors [4], as probes in scanning probe microscopy [5], or as nonbleachable biological labels [6]. Furthermore, specially engineered particles such as nanoshells are employed for photo-thermal tumor ablation and for cancer therapies [7]. Polymer nanoparticles are being used as calibration standards and, in functionalized form, also as probes in biological imaging [8]. But there are also various naturally occurring nanoparticles of high societal impact. Among them are carbon particles originating from combustion [9] or different sorts of infectious viruses [10].

Because of their small size, nanoparticles are not easy to detect and it is evident that there is high demand in novel techniques for the reliable detection, characterization, sorting, and tracking of nanoscale particles of various sorts. In public health, for example, there is concern about the impact caused by the accelerating rate of nanoparticle emissions and waste [11]. It has been determined that the inhalation of ultrafine particles originating from emissions of various kinds can cause heritable mutations [12]. The development of nanoparticle sensors is also a high priority for environmental monitoring and for the detection of various agents used in bioterrorism [13]. Furthermore, as the feature size of integrated circuits becomes increasingly smaller, contamination control of ultrafine particles poses a challenge for the semiconductor industry.

Among the different detection strategies, *optical* techniques are especially attractive because of their noninvasive nature, high-sensitivity [14], and potential for real-time detection [15]. Most of the optical schemes rely on the detection of scattered light from an ensemble of particles [16]. However, the detection of *single* nanoparticles is a challenging task which, so far, has been only accomplished by indirect means, i.e., by fluorescent labeling or immobilization on a surface and subsequent analysis with dark field microscopy [17–19]. It has been recognized that current *real-time* single particle detection methods for micrometer-sized particles are not suitable for nanoparticle detection because the intensity of light scattering scales with the sixth power of particle size. This rapid decrease of the signal renders small particles invisible.

Real-time nanoparticle detection demands an interaction mechanism with a weaker dependence on particle size. One strategy in this direction relies on detecting the scattered light interferometrically thereby accessing the scattered electric field amplitude as opposed to the scattered power. This approach has been demonstrated, almost 20 years ago, in a patent by IBM [20], and recently applied for the detection of immobilized gold particles as small as 5 nm in diameter [14]. Other detection schemes with a r_0^3 signal dependence (r_0 = particle radius) aim at measuring particle absorption cross sections by means of the photothermal effect [21] or measuring optical gradient forces acting on nanoparticles in strongly focused laser beams [15,22]. Although these methods extend the detection sensitivity to smaller particle sizes, they suffer from other shortcomings which prevent the detection of single nanoparticles in real time. Either they require particle immobilization to ensure sufficiently long acquisition times or they are subject to a background signal originating from Brownian motion or direct detector exposure.

In this Letter, we introduce a *background-free* detection approach which gives us unsurpassed real-time detection sensitivity for nanoscale particles. We demonstrate the successful detection and classification of low-index particles such as individual viruses carried in a microfluidic system. In the current version, we are able to detect individual water-solubilized polymer particles of 10 nm radius within a few milliseconds. Our detection scheme is well suited for the screening and sorting of various nanoscale particles such as viruses and larger proteins and is compatible with current microfluidic technology.

The detection scheme is schematically shown in Fig. 1(a). Using the electro-osmotic effect, a particle solution is transported through a microfluidic channel. As

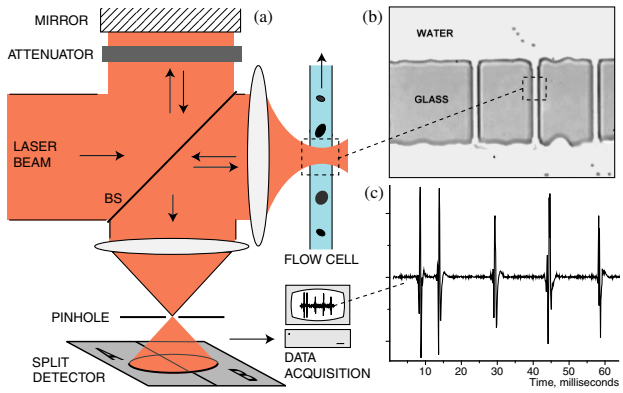

FIG. 1 (color online). Schematic rendering of the single particle detection experiment. (a) A laser beam is split by a beam splitter (BS) into a reference beam and a beam that is focused by a high numerical aperture (NA) objective (NA = 1.4) into a nanoscale channel which is part of a microfluidic system. A particle solution is transported through the channel using electroosmosis. Scattered light from a passing particle is recombined with the optionally attenuated reference beam and directed onto a split photodetector which renders a background-free signal. A pinhole (diameter = 500 microns) is used to reduce the amount of ambient light incident on the photodetector. (b) Photograph of a sequence of nanoscale channels. (c) Typical time trace of the detector signal. Individual detection events are represented by peaks with a width of a few milliseconds.

shown in Fig. 1(b), the channel is subdivided by a barrier with various nanoscale channels. A $\lambda = 532$ nm laser beam is split by a 50/50 beam splitter into two perpendicular paths. One path serves as a reference for later interferometric recombination and the other path is focused with an objective lens into a single preselected nanochannel. In principle, many channels could be sampled sequentially or in parallel by making use of a programmable spatial light modulator [23]. The lateral dimensions of the nanochannels are comparable to the size of the laser focus ensuring that no more than one particle crosses the focus at any time. The backscattered light from a particle passing through the laser focus is collected with the same objective and is then recombined with the reference beam and directed onto a split photodetector. The power of the reference beam can be arbitrarily attenuated using a $\lambda/2$ plate placed between two polarizers. Figure 1(c) shows a typical detector time trace $S(t)$. Each peak represents a single particle passing through the laser focus. The key elements in our detection scheme are (i) interferometric detection, (ii) variable attenuation of the reference beam, and (iii) the use of a split detector to ensure a background-free signal.

To understand the nature of the detector signal, let us denote the field of the scattered light as $\boldsymbol{E}_s$, and the field of the reference beam as $\boldsymbol{E}_r$. When the particle is in the focus, the intensity distribution on the detector surface is calculated as

$$I = |\boldsymbol{E}_r|^2 + |\boldsymbol{E}_s|^2 + 2\,\mathrm{Re}\{\boldsymbol{E}_r^* \boldsymbol{E}_s\}. \qquad (1)$$

The signal $S(t)$ measured by the split detector corresponds to the difference between two halves of the detector surface normalized by the total power incident on the detector, i.e., $S = (\int_{\subset} I da - \int_{\supset} I da)/\int_{\circ} I da$ with $_{\subset}$ and $_{\supset}$ denoting the two halves of the photodetector surface. In the absence of a passing particle, the reference beam and the light backreflected by optical elements are adjusted into the center of the split photodetector such that the differential signal $S(t)$ is zero. The interference between reference beam and the backreflected light does not affect our detection method because it is stationary and therefore does not generate any differential signal. Thus, $S(t)$ is a background-free signal similar to fluorescence that is commonly used to detect and track single molecules.

When a nanoparticle passes through the nanochannel, the symmetry of the backscattered light is disturbed and the detector signal $S(t)$ is defined by the interferometric term

$$S(t) = 2\mathrm{Re}\left\{\frac{\int_{\subset} \boldsymbol{E}_r^* \boldsymbol{E}_s da - \int_{\supset} \boldsymbol{E}_r^* \boldsymbol{E}_s da}{\int_{\circ} |\boldsymbol{E}_r|^2 da}\right\}. \qquad (2)$$

Here, we neglected the scattered light intensity $|\boldsymbol{E}_s|^2$ in the numerator which is legitimate as long as the reference field is stronger than the scattered field. For the same reason, we only retained the reference beam intensity $|\boldsymbol{E}_r|^2$ in the denominator and rejected all terms in $\boldsymbol{E}_s$. These approximations are justified considering the weak signal scattered by a nanoparticle.

Light scattering from a particle moving through the nanochannel depends on the particle position relative to the center of the laser focus giving rise to a nonzero signal $S(t)$ recorded by the split photodetector. The amplitude of the signal depends on the particle's polarizability which, in turn, depends on particle size and shape, as well as on its dielectric properties. As an example, Fig. 2(a) shows a histogram of signal amplitudes for a mixture of polystyrene particles of two different sizes, $r_0 = 15$ nm and $r_0 = 40$ nm. The distribution shown in Fig. 2(b) corresponds to a mixture $r_0 = 7$ nm and $r_0 = 20$ nm gold nanoparticles. The individual particle distributions appear

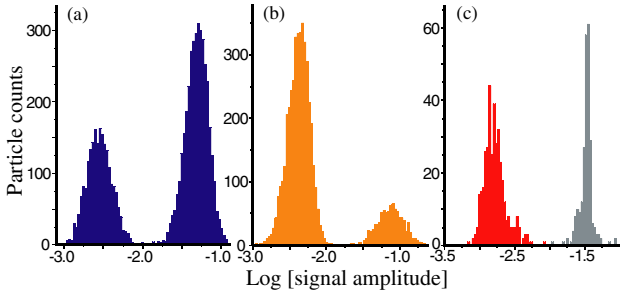

FIG. 2 (color online). Histogram of signal amplitudes for (a) a mixture of 15 nm and 50 nm polystyrene particles, (b) a mixture of 7 nm and 20 nm gold particles, and (c) a mixture of Influenza X31 virus (left peak) and 100 nm polystyrene beads. All data sets have been acquired in water with each individual detection event lasting ≈ 1 ms.

clearly resolved which demonstrates that our detection strategy is well suited for characterization and subsequent separation on a particle by particle basis. Similar procedures can be applied to separate biological particles, such as viruses or bacteria. In fact, we are currently able to detect single Influenza A X-31 viruses in real time and discriminate them from other particles of similar size [Fig. 2(c)].

To quantitatively understand the sensitivity and detection limits we first note that, for a given instant of time, the signal $S(t)$ in Eq. (2) depends linearly on the electric field amplitude E_s of the scattered light. On the other hand, the scattered field is linearly related to the amplitude of the focused laser field E_f and the particle polarizability α. Hence, the detector signal satisfies the following proportionality

$$S(t) \propto \mathrm{Re}\,(\alpha)\sqrt{P_f/P_r}, \tag{3}$$

where P_f and P_r are the powers of the focused laser beam and the reference beam, respectively. The proportionality constant depends on the momentary particle position, on the result of spatial integrations, on various physical constants, and on experimental conditions such as the numerical aperture of the objective, mirror reflectivity, detector quantum efficiency, etc. An important fact is that P_f and P_r are independent from each other. Thus, the total incident laser power can be increased and focused to a more intense spot while the reference beam can be attenuated, thereby increasing the differential signal amplitude $S(t)$ and allowing even smaller particles to be detected. Figure 3(a) demonstrates this property for a sample with $r_0 = 50$ nm polystyrene particles. The detector signal increases the more the reference beam is attenuated.

In order to assess the detection limit we analyze the signal-to-noise ratio (SNR). The noise floor of the detector signal is defined in the absence of the scattered field. Since

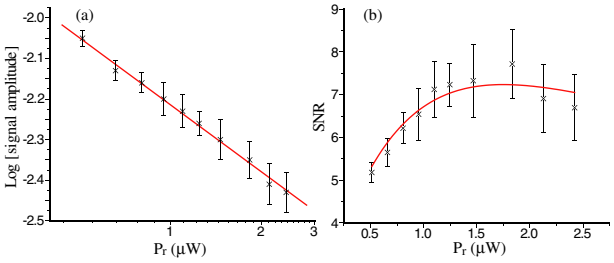

FIG. 3 (color online). Experimental analysis of detection limits using 50 nm polystyrene particles. (a) Dependence of the signal amplitude $S(t)$ on the reference beam power P_r. The red line is a fit according to Eq. (3). (b) Dependence of the signal-to-noise ratio (SNR) on the reference beam power. The red line is a fit according to Eq. (5). The measured detector noise equivalent power is $P_v = 0.7$ nW (rms), and the laser pointing instability is $\theta = 4.5 \times 10^{-4}$ (rms). These values predict a maximum at $P_r = 1.6\ \mu$W which is in agreement with the fitted curve in (b). (a),(b) Several hundreds of particles are used for each data point.

the spot of the reference beam is positioned at the center of the split photodetector, the signal noise does not depend on power noise of the laser. Instead, it is defined by the beam pointing instability and electronic noise of the detector. The pointing instability causes the beam spot to deviate from its central position on the detector giving rise to a nonzero detector response. Denoting the beam angle with respect to the unperturbed optical axis as θ the noise level for the differential signal can be expressed as

$$N = \sqrt{P_v^2 + [\theta_{\mathrm{rms}} P_r]^2}/P_r, \tag{4}$$

where P_v represents the "power equivalent" of electronic detector noise and $\theta_{\mathrm{rms}} P_r$ accounts for the pointing instability of the laser. When $P_r \gg P_v$, the noise becomes constant and proportional to θ_{rms}. However, when P_r is attenuated such that $\theta_{\mathrm{rms}} P_r \lesssim P_v$, the noise level increases rapidly with decreasing P_r. Using (3) and (4) we obtain

$$\frac{S}{N} \propto \mathrm{Re}\,(\alpha)\sqrt{\frac{P_f P_r}{P_v^2 + [\theta_{\mathrm{rms}} P_r]^2}}, \tag{5}$$

which predicts that the best SNR is achieved when the power of the reference beam is $P_r^{\max} = P_v/\theta_{\mathrm{rms}}$. Figure 3(b) shows the measured average SNR for 50 nm particles for different reference beam powers P_r. The curve demonstrates that the SNR has a maximum as predicted by Eq. (5). It turns out that the recipe for achieving the best sensitivity and lowest detection limit is to increase the laser power while keeping the reference beam at the level of maximum SNR.

The lowest possible reference beam power is determined by the backscattered light in the absence of a passing particle. This backscattered light is due to the optical index mismatch between the different interfaces and is analogous to background fluorescence in single molecule experiments. Because this backscattered light interferes with the scattered light from a passing particle it assumes a similar function as the reference beam. When this unwanted backscattering becomes stronger than the reference beam power we may simply replace P_r in Eq. (5) by the power of the backscattered light P_b and obtain the following limit $\mathrm{Max}\,[S/N] \propto \mathrm{Re}\,(\alpha)\sqrt{P_f/P_b}/\theta_{\mathrm{rms}} = \mathrm{Re}\,(\alpha) \times \sqrt{R}/\theta_{\mathrm{rms}}$ where, in the last step, we expressed the backscattered light by the focused beam power P_f using a generalized reflectivity R. Thus, the best possible SNR in our detection scheme is entirely defined by the index mismatch between the interfaces and the beam pointing instability. Both effects can be minimized in a favorably engineered detector design.

Let us now compare the SNR of our detection scheme with the SNR of standard scattering-based detection. According to Eq. (2), the maximum normalized differential signal amplitude ($S = 1$) is obtained when the phase between $\boldsymbol{E}_s$ and $\boldsymbol{E}_r$ (or $\boldsymbol{E}_b$) assumes a value which concentrates all energy on one half of the split detector. This can

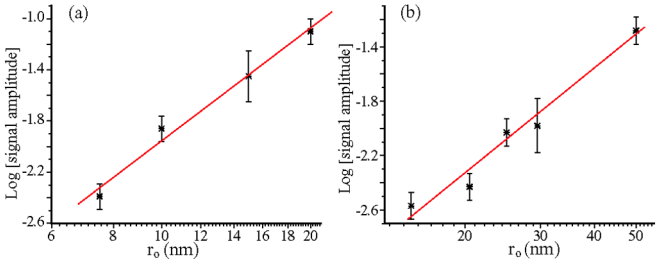

FIG. 4 (color online). Dependence of the signal amplitude on particle radius r_0 for (a) gold particles and (b) polystyrene particles in water. The red line is a fit according to r_0^n with (a) $n = 2.9 \pm 0.3$ and (b) $n = 2.6 \pm 0.3$.

only happen if the scattered field amplitude is equal to the amplitude of the reference beam or, equivalently, to the amplitude of the backscattered beam, i.e., $P_s = P_b$. For sufficiently strong powers our SNR becomes $\{S/N\}_{\text{this work}} = (1/\theta_{\text{rms}})\sqrt{P_s/P_b}$. On the other hand, the maximum SNR in standard light scattering can be written as $\{S/N\}_{\text{scattering}} = (1/\eta)P_s/P_b$, where $\eta = \sqrt{\langle dP\rangle^2}/P$ is the laser power noise. The SNR in our detection scheme is proportional to $\sqrt{P_s/P_b}$, versus P_s/P_b for scattering-based detection, and therefore proportional to the third power of particle size, versus the sixth power of particle size for scattering-based approaches. Second, the SNR in light scattering depends on laser power noise which cannot easily be controlled. On the other hand, our scheme depends on the angular pointing stability of the laser which can be controlled, for example, by reducing the optical path length. Furthermore, the dimensionless pointing stability coefficient θ_{rms} for lasers is much smaller (by orders of magnitude) than typical power noise.

In order to verify the r_0^3 dependence we measured the signal amplitudes of monodisperse particles of different sizes. As shown in Fig. 4, we obtain very good agreement with theory for both polystyrene and gold particles. The threshold for the smallest particle that can be detected is defined by the choice of the minimum acceptable SNR. As demonstrated in Fig. 2, we can reliably detect $r_0 = 15$ nm polystyrene particles and 7.5 nm gold particles in water using a SNR of 3 and a detection bandwidth of $B \approx 10$ kHz (one detection event ≈ 1 ms). By choosing a more compact design, better index matching at interfaces, and more stable laser sources we expect to considerably increase the detection thresholds.

In conclusion, we have developed a background-free, interferometric detection technique for nanoscale particles. The detector works in real time and with single particle sensitivity. Interferometric detection ensures that the signal amplitude scales with the third power of particle size and the use of a split detector ensures the best possible signal-to-noise ratio, independent of laser power noise. Within a one-millisecond time window we are able to reliably detect a single 10 nm polystyrene particle or a single 5 nm gold particle. Even higher sensitivity than reported in this Letter could be achieved by modulating the reference beam length (phase modulation) or by heterodyne detection. We expect that our detection scheme will find applications in a variety of fields such as particle tracking inside cells, detection of biowarfare agents (viruses), contamination control of water and air, and others. The detector can also be used as a prescreening stage in a larger biodetector assembly for deciding whether a subsequent one-shot detector stage with high chemical specificity (antigen-antibody, polymerase chain reaction, laser spectroscopy, etc.) should be exposed or not.

We would like to acknowledge financial support through NSF Grant No. PHS-0441964 and DARPA Grant No. MDA972-00-1-0021. We thank David Topham for providing the Influenza virus, and Matthias Danckwerts for many fruitful discussions.

*Email address: novotny@optics.rochester.edu
†Electronic address: http://www.nano-optics.org

[1] Z. Yuan *et al.*, Science **295**, 102 (2002).
[2] M. Bruchez *et al.*, Science **281**, 2013 (1998).
[3] M. Horisberger and J. Rosset, J. Histochem. Cytochem. **25**, 295 (1977).
[4] B. Dragnea *et al.*, J. Am. Chem. Soc. **125**, 6374 (2003).
[5] T. Kalkbrenner *et al.*, J. Microsc. **202**, 72 (2001).
[6] A. Schultz *et al.*, Proc. Natl. Acad. Sci. U.S.A. **97**, 996 (2000).
[7] C. Loo *et al.*, Technol. Cancer Res. Treatm. **3**, 33 (2004).
[8] R. Wiese, Luminescence **18**, 25 (2003).
[9] G. R. Cass *et al.*, Phil. Trans. R. Soc. A **358**, 2581 (2000).
[10] Center for Disease Control and Prevention Bioterrorism Agents List, http://www.bt.cdc.gov/agent/agentlist.asp
[11] R. F. Service, Science **304**, 1732 (2004).
[12] C. M. Somers *et al.*, Science **304**, 1008 (2004).
[13] M. R. Hillman, Vaccine **20**, 3055 (2002).
[14] K. Lindfors *et al.*, Phys. Rev. Lett. **93**, 037401 (2004).
[15] F. Ignatovich and L. Novotny, Rev. Sci. Instrum. **74**, 5231 (2003).
[16] N. A. Clark, J. H. Lancek, and G. B. Benedek, Am. J. Phys. **38**, 575 (1970).
[17] M. T. Blom *et al.*, Ann. Chem. **75**, 6761 (2003).
[18] A. Bouhelier, M. Beversluis, and L. Novotny, Appl. Phys. Lett. **83**, 5041 (2003).
[19] J. Prikulis *et al.*, Nano Lett. **4**, 115 (2004).
[20] J. S. Batchelder and M. A. Taubenblatt, U.S. Patent No. 5 037 202, 1991; J. S. Batchelder *et al.*, U.S. Patent No. 5 061 070, 1991.
[21] D. Boyer *et al.*, Science **297**, 1160 (2002).
[22] F. Ignatovich, A. Hartschuh, and L. Novotny, J. Mod. Opt. **50**, 1509 (2003).
[23] J. E. Curtis, B. A. Koss, and D. G. Grier, Opt. Commun. **207**, 169 (2002).